Short Communication

A Comparative Study on the Corrosion Behavior of 316L and 304 Stainless Steels in a Simulated Alkaline Environment for Lithium Extraction

Kexin Xu [1], Min Zhu[1], Jian Zhou[1,*], Fangming Shen[2], Jinjian Zhang[2], Baozhu Zhao[3]

[1] School of Mechanical Engineering & Automation, Zhejiang Sci-Tech University, Hangzhou 310018, PR China
[2] Zhejiang Quzhou Yongzheng Lithium Technology Co., LTD, Quzhou 324012, PR China
[3] CRRC Nanjing Puzhen Co., Ltd., Nanjing 210031, PR China
[*]E-mail: zmii666@126.com

The corrosion behavior of 316L SS and 304 SS in an alkaline environment of lithium extraction from salt-lake was investigated by using electrochemical measurements and immersion test. 316L SS exhibits better corrosion resistance in comparison to 304SS, which is indicated by smaller passive current density (i_p), lower carrier densities (N_D and N_A), and greater passive film resistance (R_f), as well as higher charge transfer resistance (R_{ct}). The two stainless steels occur obvious intergranular corrosion, and severe corrosion characteristics are presented inside the grain of 304 SS. The difference in the corrosion behavior of the two stainless steels are related to chemical composition, grain size, number of twins, oxide and passive film.

1. INTRODUCTION

Austenitic stainless steels of 304 and 316L are widely used in the construction field, engineering equipment, food industry, and medical instrument due to excellent corrosion resistance. [1-4]. For the wide application of the two alloys, a large amount of literature have reported the corrosion behavior and mechanism of 304 SS and 316L SS in a variety of service environments. Wang [5] investigated the microbial corrosion behavior of 304 SS and 316 SS in an anaerobic oilfield environment. It was found that the corrosion current density (i_{corr}) of 304 SS was 101 times higher than that of 316L SS, and the resistance of 316L SS to microbial corrosion was higher compared with 304 SS. The influence of chloride ion on the corrosion behavior of metals has been widely reported[6-8], and the related literature

on 304 SS and 316 SS are as follows. Martins [9] found significant corrosion of 304 SS and 316 SS helium water supply tubes due to the generation of chloride ions. Rokuro Nishimura [10] investigated the effect of chloride ion on stress corrosion cracking (SCC) behavior of 304 and 316 SS in acidic solution. The results showed that chloride ion acted as SCC promoter, and the SCC sensitivity increased with increasing chloride ion concentration. Yao [11] investigated the influence of alkaline concrete pore solution containing red mud (RM) and fly ash (FA), as well as chloride ion on the corrosion behavior of 304SS. During corrosion process, the negative charge in FA competes with Cl^- for adsorption, and thereby 304SS is more resistant to chloride ion. Through the analysis of previous research results, 304 SS and 316L SS have unique advantage in corrosion resistance under different environments.

The deterioration of the ecological environment caused by the use of fossil fuels has become one of major problems for countries around the world [12-14]. The rapid development of new energy vehicles and energy storage industry has gradually increased the demand for raw material lithium [15-17]. Currently, elemental lithium is mainly purified and processed from ores, seawater and salt-lake brines [18-20]. Lithium extraction from ores causes huge energy loss and serious environmental pollution. Seawater is inexhaustible, but the high production cost and complicated technology also hinder the industry. Therefore, lithium extraction from salt-lake brines has become an important industrial production method and has received increasing attention [19, 21]. The core of extraction is the separation of alkaline earth metal ions such as Li, Ca, and Mg from brines in salt-lakes, and the main methods used are extraction, electrodialysis, and precipitation [22-24]. At present, lithium extraction in alkaline media is the focus of research. The lix54 and Cyanex 923 synergistic solvent extraction (SSX) system developed by Pranolo et al [25] extracted 97% of the lithium from the chloride solution synthesized from the salt-lake brines in an alkaline environment, with remarkable eparation. Zhang et al. [26] used 7 (HBTA) synergistically with tri-n-octylphosphine oxide (TOPO) to extract the alkaline brine synthesized by HBTA-TOPO, which could extract 95.5% of Li. Equipments and containers may suffer severe corrosion due to strongly alkaline environment during production or experimental processes, accelerating the shortening of service life of equipment. However, the related reports on the corrosion behavior of metals in Li-containing environment are rare. Therefore, to adapt to the excellent lithium extraction technique, it is necessary to investigate the suitable materials to provide high protection for lithium extraction equipment. In this work, the corrosion behavior of 304 SS and 316L SS in a strong alkali environment containing lithium was studied by a series of corrosion tests. The results can supply a reference for the industry of lithium extraction.

2. EXPERIMENTAL

2.1. Material and solution

304 SS and 316L SS plates were cut into the samples with a dimension of 10 mm ×10 mm × 3 mm and sequentially abraded from 320 to 2000 grit SiC paper. Subsequently, they were rinsed with deionized water and alcohol, and then dried with cold air. The samples were soldered to the Cu wire and packaged with epoxy resin, exposing only a measuring surface of 1 cm^2. In this paper, 20g/L LiOH solution was employed as the simulated environment of lithium extraction from a Chinese salt-lake located in Northwest China.

2.2. Microstructural analysis

The microstructure characteristics of 304 SS and 316L SS were analyzed detailly via scanning electron microscope (SEM, FEI-quanta250), and energy dispersive X-ray spectroscopy (EDS). Before the observation, the two stainless steels were etched with aqua regia.

2.3. Electrochemical tests

The electrochemical tests were performed via a CHI660e electrochemical workstation with a conventional three-electrode system, in which 304 SS and 316L SS samples were the working electrode, saturated calomel electrode (SCE) was acted as the reference electrode, and the Pt plate as the counter electrode. The working electrode was immersed in the solution for 0.5h to ensure that a steady-state value of corrosion potential was achieved before measurement. Potentiodynamic polarization test was conducted at various solution temperatures of 35℃, 45℃ and 55℃ with a scan rate of 1 mV/s from -1 V to 0.6 V. The EIS curve was measured under an interference signal of 10 mV with a frequency range of 100 kHz ~10 mHz at open circuit potential. Before Mott-Schottky curve test, the surface passive films were grown at a constant polarized potential of 0.32 V (vs.SCE) for 2h. Then, the Mott-Schottky curve was tested at 1 kHz with a step length of 50 mV, and the potential scan range was from -1 to 0.4 V (vs. SCE).

2.4. Immersion test

Immersion test was performed with polished 304 SS and 316L SS samples, which were thoroughly washed, dried, and weighed. The two alloys were soaked in the test solution for 20 days. After the test, the specimens were taken out for rust cleaning, drying, and weighing. Subsequently, the average corrosion rates of 304 SS and 316L SS samples were calculated according to their weight loss values before and after immersion test. Finally, the corrosion characteristics of the two alloys tested in the simulated environment of lithium extraction from salt-lake were observed by SEM and stereomicroscope.

The above tests were performed at 35℃ except the potentiodynamic polarization test.

3. RESULTS AND DISCUSSION

3.1. Microstructure analysis

Fig. 1 illustrates the microstructure and EDS analysis of 304 SS and 316L SS. Both the two stainless steels mainly consist of single-phase austenite structure. 304 SS exhibits smaller grain size in comparison with 316L SS, and their average grain sizes are 10.37 μm and 15.34 μm, respectively. From Fig. 1(a,c), it is clear that twins are observed in both 304 SS and 316L SS. Nevertheless, more twins are presented in 304 SS. As compared to 316L SS, some white fine particles (such as the black dashed circle

range) are randomly distributed on the surface of 304 SS in Fig. 1(a). And there are no obvious particles existing in 316L SS.
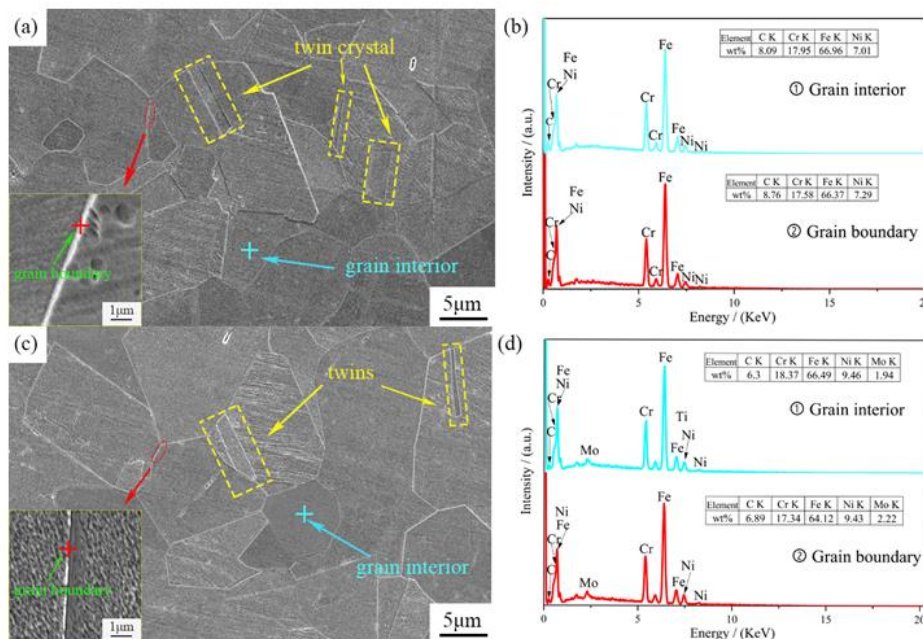

Figure 1. Microstructure and EDS result of 304 SS (a,b) and 316L SS (c,d)

Fig. 1(b,d) displays the EDS results of grain interior and grain boundary (GB) of 304 SS and 316L SS, indicating that the contents of major alloying elements of Cr and Fe are approximately the same. However, 316L SS has about 2% Mo, and more Ni content than those of 304 SS. Additionally, for the two alloys, the Cr content at grain boundary is slightly lower than that in the internal of grain. This may be due to the fact that the diffusion rate of Cr within the grain is less than that along the grain boundary [27-28].

Further analysis of the white particles in Fig.1(a) was performed by EDS. As shown in Fig. 2, white spherical particles distributed nearly GB regions are defined as oxides containing O, Al, Ti, C, Cr, Co, Ni, Mn, Mg, Ca, and Fe.
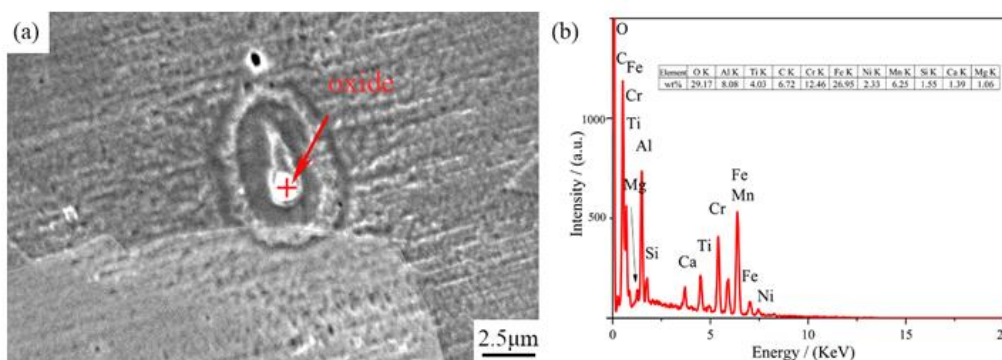

Figure 2. morphology (a) and EDS result (b) of oxide within 304 SS

3.2. Electrochemical measurements

Fig. 3 exhibits the potentiodynamic polarization curves of 304 SSL and 316L SS in LiOH solution. The similar passive characteristics imply that passive films are generated on the surfaces of two alloys. This may be attributed to the fact that the two stainless steels have the similar elemental composition (Fig. 1(b,d)) and they are covered with a passivation film containing chromium [29-30]. In Fig. 3(d), as solution temperature increases, the i_p values of the two alloys increase, and 316L SS exhibits lower i_p at various temperatures, compared with those of 304 SS. In general, the i_p reflects the corrosion rate of passivated metals. The larger i_p means the greater dissolution rate of passive film [31-32]. Hence, the corrosion resistance of 316L SS in LiOH solution is better than that of 304 SS. Furthermore, an increased temperature decreases the passivity and corrosion resistance of the two metals indicated by the change tendency of i_p.
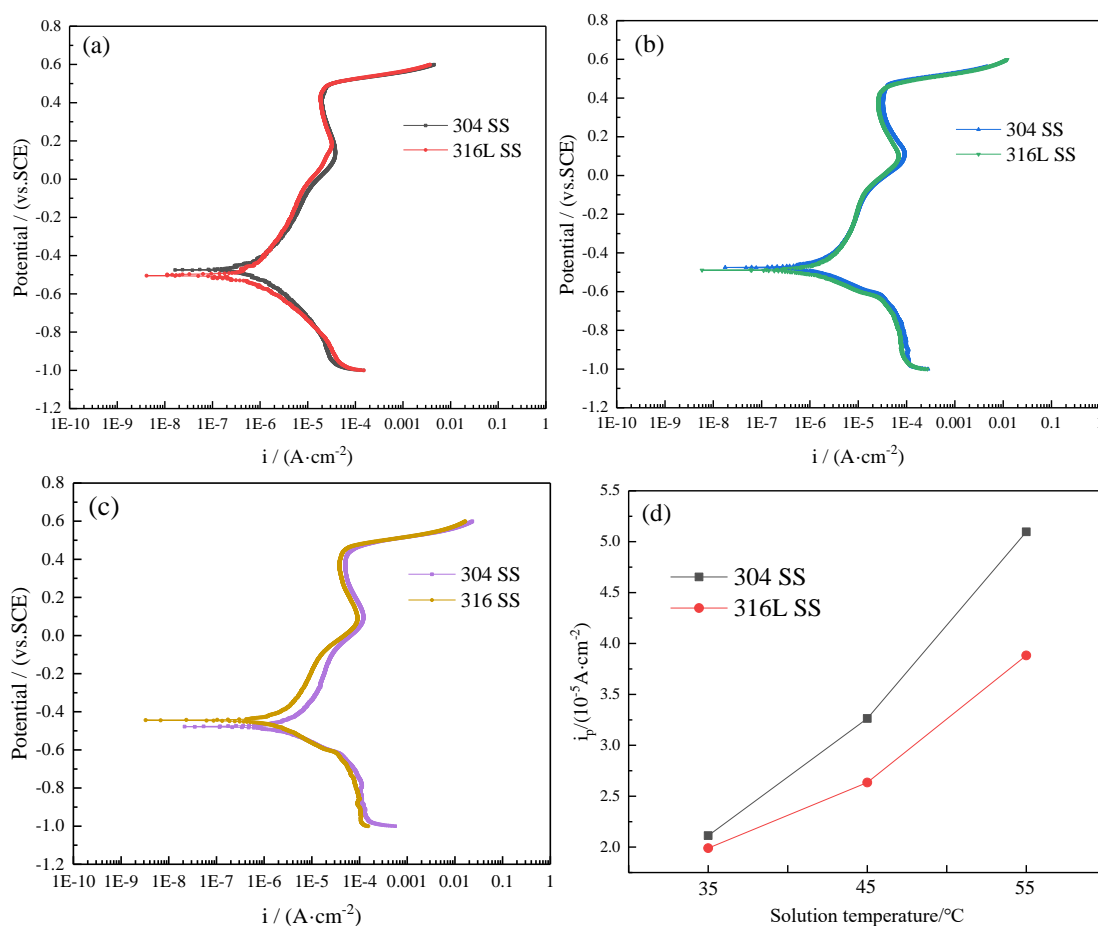

Figure 3. Potentiodynamic polarization curves of 304 SS and 316L SS in a simulated alkaline environment for lithium extraction at different temperatures: (a) 35°C; (b) 45°C; (c) 55°C; (d) fitted ip values.

The influence of temperature on the corrosion resistance of the two stainless steels is inversely proportional, which can be analyzed from several respects. On the one hand, the dissolved oxygen content decreases with the increase of temperature. When the oxygen content is lower than the critical value, there is no enough oxygen to involve in the cathodic reaction, and the corrosion process is inhibited [33]. On the other hand, the increase of temperature causes an increase in the defects inside the passivation film. Additionally, the diffusion coefficient of the solution ions increases as the temperature rises[34]. The penetration ability of harmful ions to the passivation film is enhanced, thus it is more likely to generate pitting corrosion and deterioration of corrosion resistance of the two alloys at higher temperature.

The Nyquist and Bode plots for 304 SS and 316L SS tested in LiOH solution are presented in Fig. 4. In Fig. 4a, two curves present incomplete capacitive characteristics. 316L SS exhibits the larger radius of capacitive arc. The difference in the charge transfer between the two phases of electrolyte/electrode causes different arc radius [35]. The larger the radius, the better the corrosion resistance is. In Fig. 4(b), it is observed that the impedance modulus of 316L SS is greater than that of 304 SS in the low-frequency range (0.01 Hz < f < 1 Hz). Combining with the curves in Fig.3, the above characteristics imply that the resistance of the metal to polarization is influenced by the performance of passive film [36]. Thus, 316L SS has superior passive film property. Moreover, the phase angle of 316L SS is larger than that of 304 SS in the medium frequency range with a maximum value of 84° as displayed in Fig 4(c). The larger phase angle reflects the stronger protection of the passive film [37]. In summary, a more stable and high protective passive film is produced on the 316L SS, which improves its anti-corrosion property. This is consistent with the results of potentiodynamic polarization curve.

To intuitively compare the corrosion resistance of 304 SS and 316L SS, the measured EIS data was further fitted and analyzed using an equivalent circuit (Fig. 5). In the equivalent circuit diagram, R_s is the solution resistance; R_f is the passive film resistance; R_{ct} is the charge transfer resistance (solution/substrate); Q_f denotes the passive film capacitance, and Q_{dl} is the non-ideal electric double layer capacitance. The corresponding fitted values for each component are presented in Table 1. A significant difference between 304 SS and 316L SS is emerged. Obviously, the R_f and R_{ct} of 316L SS are greater, with the R_{ct} value of 316L SS being an order of magnitude more than 304 SS. Furthermore, 316L SS possesses the lower Q_f. Generally, the larger R_f and smaller Q_f indicate the less defects in the dense passive film [38]. Additionally, the reciprocal magnitude of R_{ct} ($1/R_{ct}$) can characterize the corrosion rate. The greater the $1/R_{ct}$, the larger the corrosion rate is [39]. Hence, 316L SS exhibits better anti-corrosion performance.
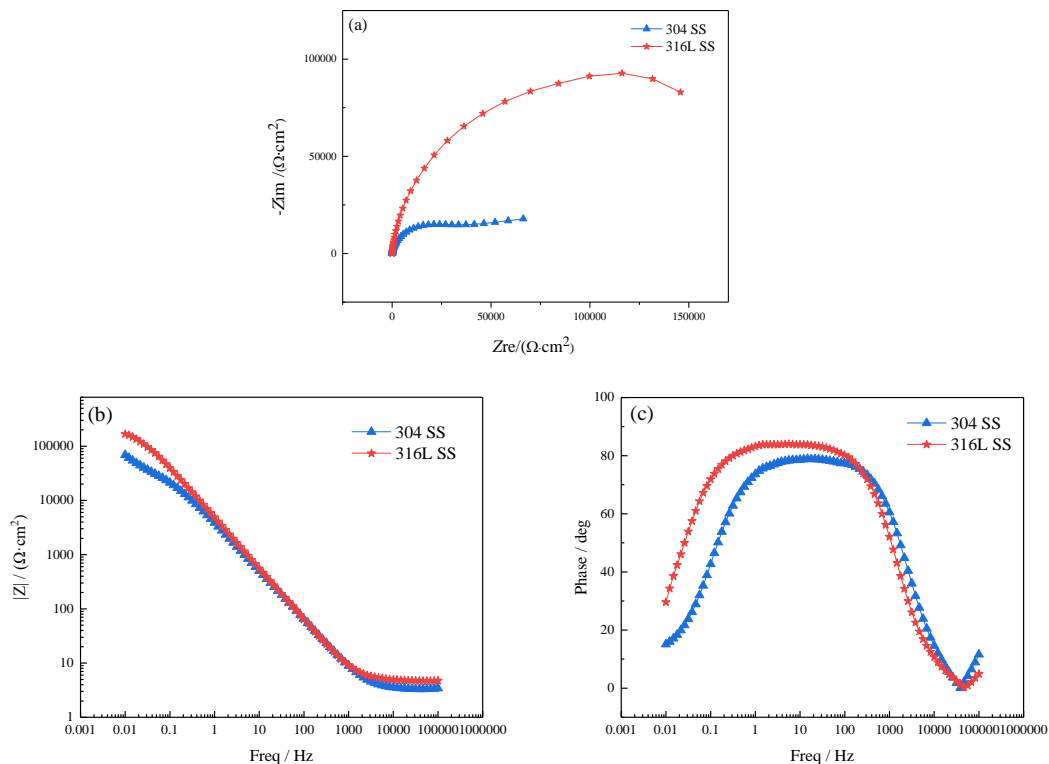
Figure 4. EIS curves of 304 SS and 316L SS in a simulated alkaline environment for lithium extraction at 35°C: (a) Nyquist plots; (b, c) Bode plots.
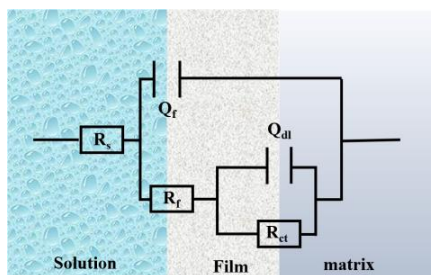

Figure 5. Equivalent circuit for fitting EIS data.

Table 1. The fitted electrochemical parameters for EIS data tested in a simulated alkaline environment for lithium extraction at 35°C.

SS	R_s （$\Omega\cdot cm^2$）	Q_f （$10^{-5}\,\Omega^{-1}\,s^n\cdot cm^{-2}$）	R_f （$10^4\,\Omega\cdot cm^2$）	Q_{dl} （$10^{-5}\,\Omega^{-1}\,s^n\cdot cm^{-2}$）	R_{ct} （$10^4\,\Omega\cdot cm^2$）
304 SS	3.316	4.663	1.538	2.562	3.642
316L SS	4.797	3.660	3.673	1.393	17.470

The semiconductor properties of passive films grown on 304 SS and 316L SS were investigated by the Mott-Schottky curve. The relationship between the space charge capacitance (C) and the applied electrode potential (E) can be expressed by Formula 1 [40].

$$\frac{1}{c^2} = \pm \frac{2}{\varepsilon \varepsilon_0 e N} \left(E - E_{fb} - \frac{\kappa T}{e} \right) \qquad (1)$$

The positive and negative slopes of the Mott-Schottky curve correspond to the "+" and "-" signs in the above formula, indicating the n-type or p-type semiconductor characteristics of passive film. The donor (N_D) and acceptor (N_A) densities were obtained from the slopes of the curves. In addition, ε is the dielectric constant (15.6) [41], ε_0 is the vacuum dielectric constant (8.854×10^{-12} F·m^{-1}), e is the electron charge (1.602189×10^{-19} C), N denotes the carrier density, K represents the Boltzmann constant (1.38×10^{-23} J·K^{-1}), and T denotes the absolute temperature. E is the applied electrode potential and E_{fb} is the flat-band potential.
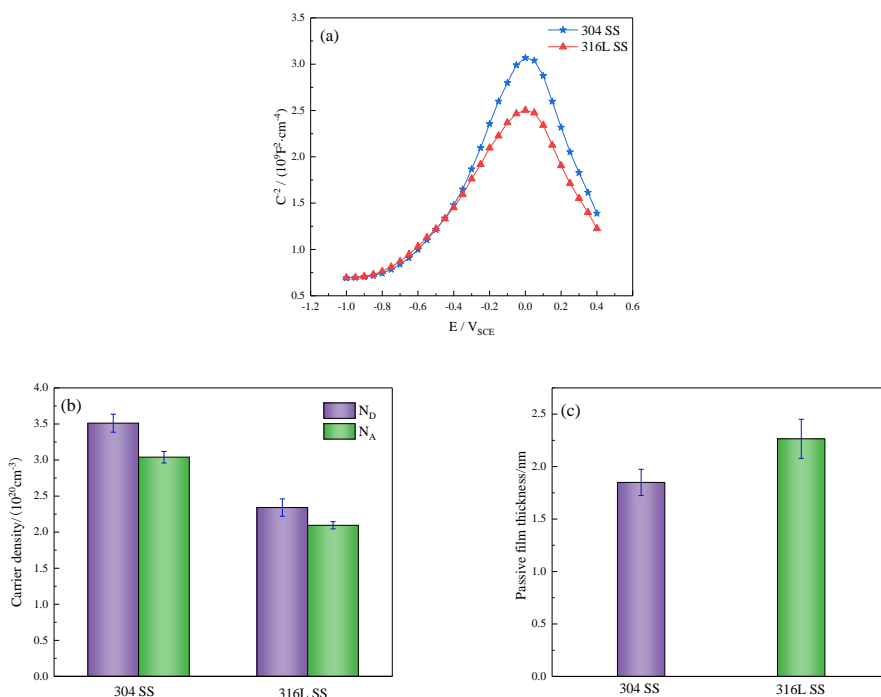

Figure 6. Mott-Schottky plots (a), carrier density (b), and thickness of passive films (c) produced on the two stainless steels at a passive potential of 0.32 V for 2 h.

Fig. 6(a) exhibits the Mott-Schottky curves of 304 SS and 306L SS, and the two curves exhibit similar shapes. In the whole potential range, the curves can be divided into two segments. As the voltage increases, the composition and structure of the passive film changes, which can be reflected by the variation in the slope of the curve. The N_D and N_A are the structural defects within the crystals, and the degree of defects in the passive film can be reflected by their values [42]. Fig. 6(b) exhibits the N_D and N_A values of 304 SS and 316L SS. According to the histogram, it is found that the N_D and N_A values of 316L SS are smaller in comparison with 304 SS, which indicates that the passive film of 316L SS is denser, which can prevent harmful ions from passing through the passive film and avoid the solution

directly contact with the substrate, resulting in the lower pitting sensitivity [43-44]. The passive film thickness (d) was calculated by Formula 2.

$$d = \left[\frac{2\varepsilon\varepsilon_0\left(E - E_{fb} - \frac{\kappa T}{e}\right)/e}{eN_D}\right]^{1/2} \qquad (2)$$

Fig. 6(c) shows the difference in the thickness of passive films of the two stainless steels. For 304 SS, the thinner passive film is easy to dissolve and rupture, hence its protection is weaker than 316L SS.

3.3. Immersion test

Fig. 8 displays the corrosion characteristics of 304 SS and 316L SS immersed in LiOH solution for 20 days. In Fig. 8, significant intergranular corrosion occurs in both 304 SS and 316 L SS. On the surface of corroded 304 SS, large-sized corrosion pits appear and dense pinhole pits are distributed at their bottom. A great amount of pits with different sizes are generated around GB regions. Moreover, severe pitting characteristics are observed in the interior of grains. Some pits gradually fuse and develop into larger size one. Compared to 304 SS, 316L SS exhibits a slighter corrosion status, with less small pits occurred inside of grains. Fig. 7 shows the average corrosion rates of 304 SS and 316L SS, with 304 SS showing a significantly higher corrosion rate, which corresponds to the corrosion morphologies of the two alloys after immersion shown in Fig. 8.
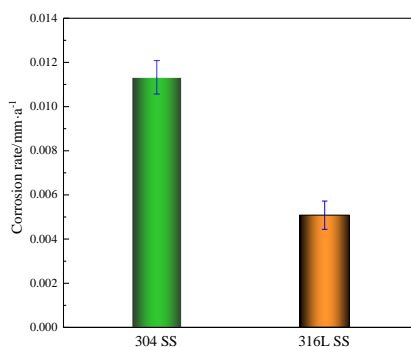

Figure 7. Corrosion rates of 304 SS and 316L SS immersed in a simulated alkaline environment for lithium extraction at 35°C for 20 days

Differences in microstructure can affect the corrosion resistance of alloys. It is well known that GB possesses irregular atomic arrangement, high dislocation density, and uneven element distribution. In addition, many defects and impurities are easily aggregated at GB areas [45]. Thus, the high electrochemical activity of GBs results in the preferential destruction of passive film located at these regions, and the direct contact of harmful ions in solution with GB through defects of passive film leads to the occurrence of intergranular corrosion. By comparing the amount of twins in Fig. 1(a,c), more twins are presented in 304 SS. The twin regions are susceptible to corrosion due to high atomic energy and

electrochemical activity [46]. In addition, many literature have reported that large grain size can promote the anti-corrosion property of metals[47-48]. Therefore, 316L SS exhibits superior corrosion resistance.
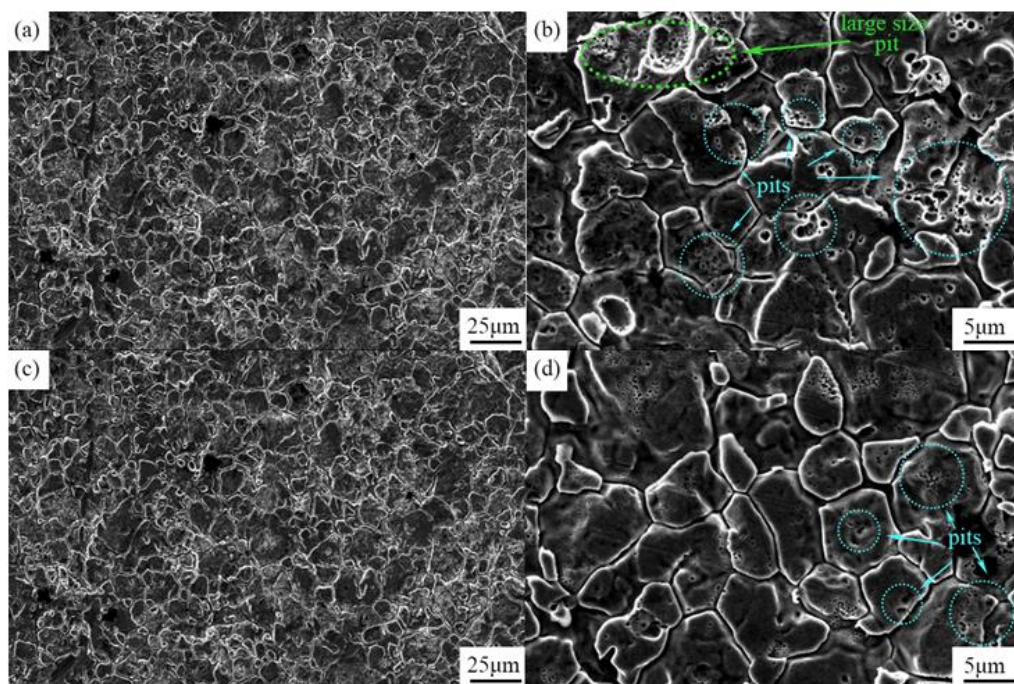

Figure 8. Corrosion morphologies of 304 SS and 316L SS immersed in a simulated alkaline environment for lithium extraction at 35°C for 20 days: (a,b) 304 SS; (c,d) 316L SS

As shown in Fig. 2, it is found that oxides containing C and Cr are located near the grain boundaries of 304 SS. The formation of oxides causes the Cr content at the grain boundaries (Fig. 1(b,d)) to be slightly lower than that in the grain interior. This phenomenon has been mentioned in the following studies. Meng [49] calculated that the diffusion energy of Cr element at grain boundaries is 162-252 kJ/mol, while its diffusion energy inside the grains is 540 kJ/mol, and confirmed that elemental Cr more readily precipitates on GB regions and forms carbides or oxides. The appearance of Cr-depleted grain boundaries causes a decrease in the homogeneity and stability of the passive film grown on the surface of alloys. Furthermore, Kondo, Tsisar, and Kimura et al [50-52] verified that the precipitated carbides positively contributed to the selective dissolution of the substrate adjoining the GB. Consequently, Cr depletion at GBs is one of the main causes of intergranular corrosion.
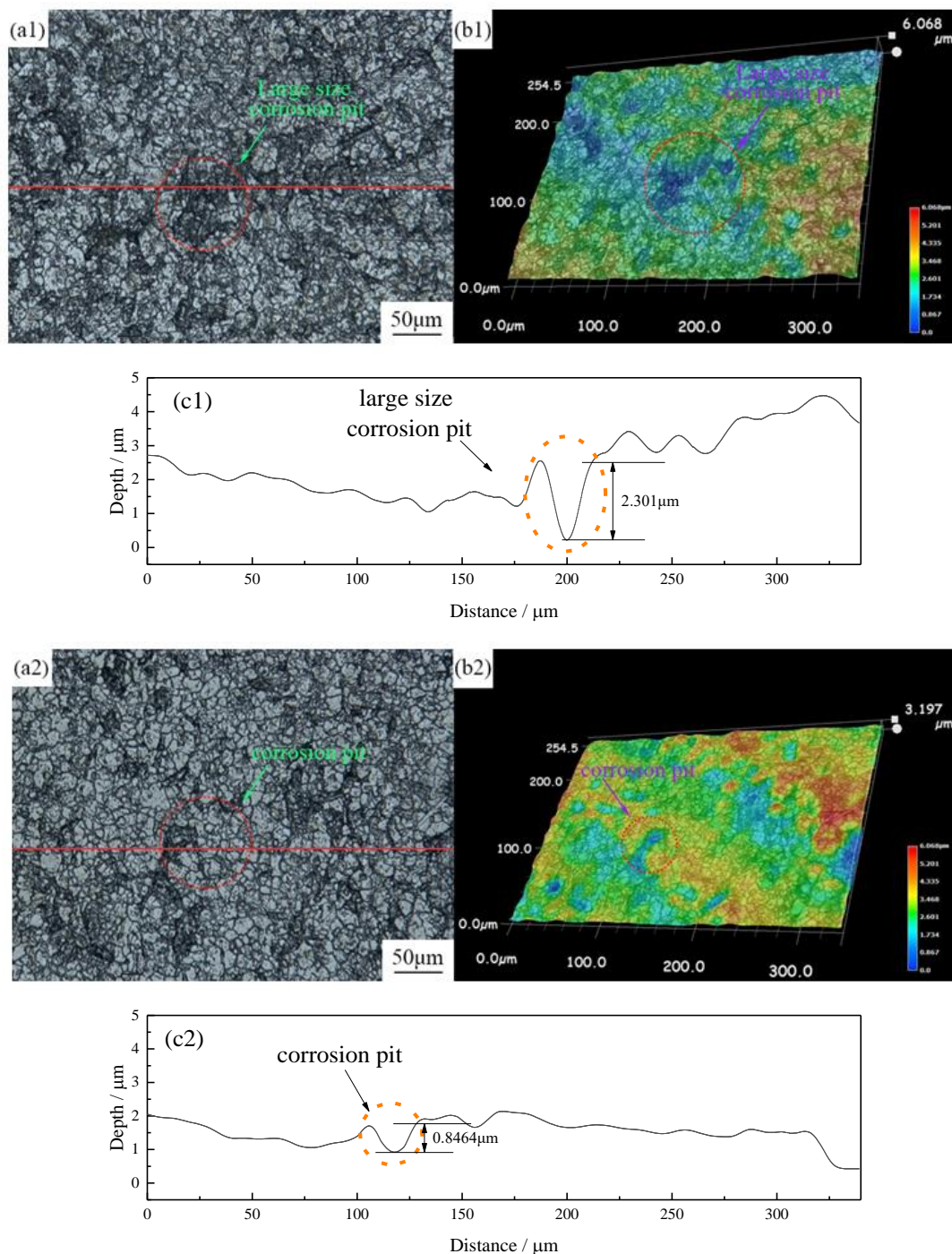
Figure 9. Corrosion morphologies of 304 SS and 316L SS immersed in a simulated alkaline environment for lithium extraction at 35°C for 20 days: (a1,b1) 2D and 3D of 304 SS; (a2,b2) 2D and 3D of 316L SS; (c1,c2) the corresponding data.

Fig. 9 illustrates the two/three-dimensional corrosion morphologies of the two stainless steels immersed in LiOH solution for 20 days, which shows obvious intergranular corrosion characteristics. Fig. 9 (c1,c2) reveals the height variation of the section where the straight lines located in Fig.9 (a1,a2). By comparing with 316L SS, 304 SS exhibits the distinct depth change, with some larger and deeper corrosion pits. Known from the above results, 316L SS possesses better anti-corrosion resistance in comparison to 304SS.

Except for the grain size and the amount of twins, the difference in the corrosion behavior of the two stainless steels is also attributed to different contents of Mo and Ni in their matrix. The related reports pointed out that Mo improved the compactness of passivation film and inhibited the occurrence of pitting [53-54]. Wu [55] found that Ni combined with anions in solution while enriching passivation film, preventing harmful ions from penetrating passivation film. Thus, by contrast with 304 SS, higher contents of Mo and Ni increase the anti-corrosion resistance of 316L SS. Additionally, according to the EDS results in Fig. 1, the pitting resistance equivalent number (PREN = wt.% Cr + 3.3-wt.% Mo + 16-wt.% N) was calculated to explain the difference in the susceptibility to pitting corrosion [56]. The larger the PREN, the higher the pitting resistance is [57]. In this text, the PREN value of 316L SS (24.73) is nobler than that of 304 SS (17.95). In addition, for 304 SS, the presence of oxides near grain boundaries accelerates the occurrence of pitting corrosion. Due to different corrosion potentials between the oxide and the matrix, the oxide may act as the cathode and the matrix serves as the anode, which induces local micro-galvanic corrosion. The electrochemical stability near the oxide is disrupted, increasing the susceptibility to pitting corrosion [58]. Meanwhile, the physical properties of oxide and matrix are different, hence, the internal stresses generated by the formation of oxides causes lattice distortion of the grains [59], decreasing the pitting resistance of 304 SS. The smaller grain size of 304 SS means a higher percentage of grain boundaries. The high activity of GBs leads to poorer stability of the passivation film in their vicinity. As the percentage of GB increases, the pitting-sensitive areas increase, thus pitting is more likely to occur inside the grain regions close to the GBs. Consequently, severe corrosion characteristics are exhibited inside the grains of 304 SS.

4. CONCLUSIONS

The corrosion behavior of 316L SS and 304 SS in an alkaline environment of lithium extraction from salt-lake was studied, and the main conclusions are as follows:

1.   In LiOH solution, 316L SS possesses better anti-corrosion resistance in comparison to 304SS.

2.   Polarization curves reveal that the increasing solution temperature reduces the passivity and corrosion resistance of the two alloys.

3.   The two stainless steels exhibit obvious intergranular corrosion, and severe corrosion characteristics are presented inside the grains of 304 SS. The difference in the corrosion behavior of the two stainless steels are related to chemical composition, grain size, number of twins, oxide and passive film.

References

1.   J.Xu, S.G. Wu, J.P Han, J.J. Wang and Z.J. Li, *J. Constr. Steel. Res.,* 192 (2022) 107219.

2. Z.H. Sun, M. Moradi, Y.X. Chen, R. Bagheri and C. Xu, *Mater. Chem. Phys.,* 208 (2018) 49.
3. Q.F. Wang, M.X. Zhang, C.T. Yang, Y. Yang, E.Z. Zhou, P. Liu, D.Q. Jin, D.K. Xu, L. Wu and F.H. Wang, *J. Mater. Sci. Technol.,* 128(2022)118.
4. Y.C. Tang, S.J. katsuma, S.J. Fujimoto and S. Hiromoto, *Acta. Biomater.,* 2 (2006) 709.
5. D. Wang, R. Jia, S. Kumserranee, S. Punpruk and T.Y. Gu, *Eng. Failure Anal.,* 122 (2021) 105275.
6. L.W. Wang, J.M. Liang, H. Li and Z.Y. Cui, *Corros. Sci.*, 178 (2021) 109076.
7. H.L. Liao, J.C. Lin and S.L. Lee, *Corros. Sci.,* 51 (2009) 209.
8. W.M. Tian, N. Du, S.M. Chen and Q.Y. Wu, *Corros. Sci.,* 85 (2014) 372.
9. C.M.B. Martins, J.L. Moreira and J.I. Martins, *Eng. Failure Anal.,* 39 (2014) 65.
10. R. Nishimura, *Corros. Sci.,* 34(1993) 1859.
11. N. Yao, X.C. Zhou, Y.Q. Liu and J.J. Shi, *Cem. Concr. Compos.,* 132 (2022) 104637.
12. J.B. Goodenough and K.S. Park, *J. Am. Chem. Soc.*, 135 (2013) 1167.
13. L Ma, T.G. Yu, E. Tzoganakis, K. Amine, T.P. Wu, Z.W. Chen and J Lu, *Adv. Energy Mater.,* 8 (2018) 348.
14. M.S. Shahjalal, P.K. Roy, T. Shams, A. Fly, J.I.chowdhury, M.R. Ahmed and K. Liu, *Energy,* 241 (2022) 122881.
15. Y. Polishchuk, E. Shembel, A.S. Fedorkova, A. Markevich, V. Redko and I. Lysytsya, *Mater. Today: Proc.,* 50 (2022) 430.
16. J.L. Hu, Q.Q. Chen, Q. Xia and L.Z Zhang, *Appl. Surf. Sci.,* 599 (2022) 153951.
17. G. Ahmed, Z.H. Awan, F.A. Butt, F. Raza, S. Hashmi, G. G. Kumar and M. Christy, *J. Power Sources,* 538 (2022) 231379.
18. S.X. Yang, F. Zhang, H.P. Ding, P. He and H.S.Zhou, *joule,* 2 (2018)1648.
19. S.N. Lin, T.A. Zhang, X.J. Pan and J.J. Zhang, *J. Clean. Prod.,* 327 (2021) 129481.
20. G. Liu, Z.W. Zhao and L.H. He, *Desalination,* 474 (2020) 114185.
21. D.Q. Li, Q.G. Liu and Ah. Ghahremanb, *Hydrometallurgy,* 187 (2019) 81.
22. Y. Zhang, Y.H. Hu, L. Wang and W. Sun, *Miner. Eng.,* 139 (2019) 105868.
23. L.C. Zhang, J.F. Li, R.R. Liu, Y.Q. Zhou, Y.Z Zhang,L.M. Ji and L.J Li, *J. Mol. Liq.*, 362 (2022) 119667.
24. Y.B. Qiua, L. Yaoa, C. Tanga, Y. Zhaob, J.J. Zhua and J.N. Shen, *Desalination,* 406 (2019) 1.
25. Y. Pranolo, Z.W. Zhu and C.Y. Cheng, *Hydrometallurgy,* 154 (2015) 33.
26. L.C. Zhang, L.J. Li, D.Shi, J.F. Li, X.W. Peng and F. Nie, *Sep. Purif. Technol.,* 188 (2017) 167.
27. P. Moulin, A.M Huntz and P. Lacombe, *Acta Metall.Sin.,* 27 (1979) 1431.
28. S.Rajeshwari K, S.Sankaran, K.C. Hari Kumar, H.Rösner, M. Peterlechner, V.A. Esin, S. Divinski and G. Wilde, *Acta Materialia*, 195 (2020) 501.
29. H. Springer, C. Baron, L. Tanure and M. Rohwerder, *Mater. Today Commun.,* 29 (2021) 102947.
30. X.J. Yang, Y.Yang, M H. Sun, J.H. Jia, X.Q. Cheng, Z.B. Pei, Q. Li, D. Xu, K. Xiao and X.G. Li, *J. Mater. Sci. Technol.,* 104 (2022) 67.
31. C.H. Tsau, M.C. Tsai and W.L. Wang, *Materials,* 15 (2022) 888.
32. A.Q. Fu, and Y.F. Cheng, *Corros. Sci.,* 52 (2010) 2511.
33. X.H. Nie, X.G. Li, C. W. Du, Y. F. Cheng, J Appl Electrochem, (2009) 39:277–282.
34. J. Qiu, Y.H Li, Y Xu, A.J Wu, D.D Macdonald, Corros Sci, 175 (2020) 108886.
35. C.N. Cao, *Electrochim. Acta,* 35 (1990) 831.
36. H. Luo, H.Z. Su, B.S. Li and G.B. Ying, *Appl. Surf. Sci.,* 439 (2018) 232.
37. W.R. Wang, J.Q. Wang, Z.H. Sun, J.G. Li, L.F. Li, X. Song, X.D. Wen, L. Xie and X. Yang, *J. Alloys Compd.,* 812 (2020) 152139.
38. H.C. Tian, X.Q. Cheng, Y. Wang, C.F. Dong and X.G. Li, *Electrochim. Acta,* 267 (2018) 255.
39. M.X. Guo, J.R. Tang, C. Peng, X. H. Li, C.Wang, C. Pan and Z.Y. Wang, *Mater. Chem. Phys.,* 276 (2022) 125380.
40. M. Sanchez, J. Gregori, C. Alonso, J.J. García-Jare, H. Takenouti and F. Vicente, *Electrochim.*

Acta, 52 (2007) 7634.
41.   R.M. Fernández-Domene, E. Blasco-Tamarit, D.M.García-García and J. García-Antón, *Electrochim. Acta*, 95 (2013) 1.
42.   R.Babic, M.Metikos-Hukovic, *J. Electroanal. Chem.,* 358 (1993) 143.
43.   S. Ahn, H.S. Kwon, Macdonald and D.D. Macdonald, *J. Electrochem. Soc.,* 152 (2005) B482.
44.   M. Zhu and C.W. Du, *J. Mater. Eng. Perform.,* 26 (2016) 221.
45.   G.L. Song and Z.Q. Xu, *Corros. Sci.,*54 (2012) 97.
46.   H.L. Yan, J.Q. Wang, Z.M. Zhang and B.O. Okonkwo, *J. Mater. Sci. Technol.,* 122 (2022) 219.
47.   W.J. Zhang, F.G. Liu, L.X. Liu, Q.G. Li, L.Y.Liu, F.C. Liu and C.P. Huang, *Mater. Today Commun.,* 31 (2022) 103723.
48.   K.D. Ralston, N. Birbilis and C.H.J. Davies, *Scr. Mater.,* 63 (2010) 1201.
49.   X Meng, G Zuo, J Ren, W Xu, Z Sun, M Huang, W Hu, J Hu and H Deng, *J. Nucl. Mater.,* 480 (2016) 25.
50.   M. Kondo, M. Takahashi, T. Tanaka, V. Tsisar and T. Muroga, *Fusion Eng. Des.,* 87 (2012)1777.
51.   V. Tsisar, M. Kondo, Q. Xu, T. Murog, T. Nagasaka and O. Yeliseyeva, *J. Nucl. Mater.,* 417 (2011) 1205.
52.   A. Kimura, R. Kasada, A. Kohyamaa, S. Konishi and M. Enoeda, *Fusion Eng. Des.,* 81 (2006) 909.
53.   H. Savaloni and M. Habibi, *Appl. Surf. Sci.,* 258 (2011) 103.
54.   A. Pardo, M.C. Merino, A.E. Coy, F. Viejo, R. Arrabal and E. matykina, *Corros. Sci.,* 50 (2008)780.
55.   W. Wu, Z.P. Zeng, X.Q. Cheng, X.G. Li and B. Liu, *J. Mater. Eng. Perform.,* 26 (2017) 6075.
56.   L.D. Chen, H. Tan, Z.Y. Wang, J. Li and Y.M. Jiang, *Corros. Sci.,* 58 (2012) 168.
57.   B. Deng, Z.Y. Wang, Y.M. Jiang, T. Sun, J.L. Xu and J. Li, *Corros. Sci.,* 51 (2009) 2969.
58.   M. Zhu, F. He, Y.F. Yuan, S.Y. Guo and J. Pan, *Intermetallics,* 139 (2021) 107370.
59.   Y.H. Zhang, Q. Hu, M.J. Dai, F. Huang, F.Y. Cheng and J. Liu, *Mater. Corros.*, 71(2019)876.